Steel and Composite Structures, *Vol. 28, No. 2* (*2018*) *149-165*
DOI: https://doi.org/10.12989/scs.2018.28.2.149

Nonlinear free and forced vibration analysis of microbeams resting on the nonlinear orthotropic visco-Pasternak foundation with different boundary conditions

Ali Ghorbanpour Arani [*1,2] and Farhad Kiani [1a]

[1] *Department of Mechanical Engineering*, *University of Kashan*, *Kashan*, *Iran*
[2] *Institute of Nanoscience& Nanotechnology*, *University of Kashan*, *Kashan*, *Iran*

(*Received June 8, 2017, Revised October 25, 2017, Accepted May 24, 2018*)

Abstract. Using the modified couple stress theory and Euler-Bernoulli beam theory, this paper studies nonlinear vibration analysis of microbeams resting on the nonlinear orthotropic visco-Pasternak foundation. Using the Hamilton's principle, the set of the governing equations are derived and solved numerically using differential quadrature method (DQM), Newark beta method and arc-length technique for all kind of the boundary conditions. First convergence and accuracy of the presented solution are demonstrated and then effects of radius of gyration, Poisson's ratio, small scale parameters, temperature changes and coefficients of the foundation on the linear and nonlinear natural frequencies and dynamic response of the microbeam are investigated.

Keywords: microbeam; nonlinear vibrations; modified couple stress theory; orthotropic visco-Pasternak

1. Introduction

Nowadays, research and studies on micro/nano-electro-mechanical (MEMS/NEMS) systems are growing significantly. These microbeams can be used in atomic force microscope, microswitch (Ghayesh *et al*. 2014), micro-sensors, accelerometers, electrostatic micro-actuators and micro- pumps (Rashvand *et al*. 2013). The use of MEMs in science and engineering fields, such as biomedical engineering, optics, aerospace industry and smartphones, is extensive. The physical dimensions of the microbeams used in MEMs and NEMs are from sub-microns to one millimeter (Lyshevski 2002). It has been proven experimentally that the effect of size on mechanical behaviour of a microbeam is important when its dimensions are micron and sub-micron (Mohammadimehr and Shahedi 2016). According to the reports in the experimental trials it has been observed that by reducing the diameter and thickness in the twisting and bending test for the sub-micron and micron size ranges, the phenomenon of hardening unexpectedly occurs and the classical theories of elasticity cannot analyse it (Stölken and Evans 1998, Simsek 2011). For this reason, the analysis of mechanical behavior of structures in the range of micron is inevitable. Therefore, different experimental and thesaurus studies have been conducted to measure the natural frequency. Some of these studies include determining the natural frequency of the microbeams in vacuum and electrical measurement methods to obtain resonant frequency (Tilmans and Legtenberg 1994). Micro and sub-micron experiments are difficult and expensive. Therefore, suitable mathematical models for microstructure are presented, and researchers have used analytic, semi-analytic and numerical models (Mohammadimehr *et al*. 2016). However, behaviours relating to micro and submicron scale are not predictable and cannot be explained by classical continuum mechanics. Therefore, non-classical continuous theories were presented during the past few decades, including nonlocal theory of elasticity (Eringen and Edelen 1972). According to this theory, stress at a point not only depends on the strain at the same point, but also depends on strain in other parts of material. (Ghorbanpourarani Arani *et al*. 2010). Also, according to this theory, extensive researches have been conducted on nonlinear Euler-Bernoulli beam model by carbon nanotubes (Tagrara *et al*. 2015). Another theory includes the theory of surface tension effects for material at micro and nano scale (Gurtin and Ian Murdoch 1975). Sahmani *et al*. (2014) conducted nonlinear vibration analysis for thin-walled beams by combining Galerkin method and DQM. They also discussed the effect of softening and hardening behaviours of beams. The strain gradient can be mentioned as another theory. In this theory four constant materials (two constant classic numbers and two additional constant numbers) for micro material have been considered. This theory has tensors of higher order such as Curvature gradient tensor, deviatory stretch gradient tensor and symmetric rotation gradient tensor. Ghorbanpour Arani *et al*. (2013) used strain gradient theory to investigate free vibration and stability of Euler-Bernoulli microbeam based on Pasternak foundation. Yang *et al*. (2002) offered a

∗Corresponding author, Full Professor,
E-mail: aghorban@kashanu.ac.ir;
a_ghorbanpour@yahoo.com
[a] Ph.D. Student, E-mail: kiani@shaiau.ac.ir

http://www.techno-press.org/?journal=scs&subpage=6
ISSN: 1229-9367 (Print), 1598-6233 (Online)

more specific mode of strain gradient theory which only needed an additional constant related to length scale parameter. This mode is called modified couple stress theory (MFSDT). Different tests were conducted to determine length scale parameter in the modified couple stress theory which includes tests of twisting and bending and stretching microbeams (Lam *et al*. 2003). In this theory, strain energy density function depends on the strain tensor and the symmetric part of the curvature tensor. Moreover, due to the rotational effects and curve in the rotational gradient tensor, this theory has a good accuracy for materials at the micron scale. Yang *et al*. (2012) examined electrodynamic response of a microbeam. To do so, they considered the initial curve and nonlinear deformation, and they showed that as the length increases, the importance of studying the nonlinear frequency increases. Roque *et al*. (2013) studied static bending of composite beam Timoshenko with simple support using modified couple stress theory and meshless numerical method based on the order related to the radial basis functions. Kong *et al*. (2008) examined effects of the small-scale parameter on frequency ratio (linear frequency of the nonlocal to the linear frequency of the local). By choosing two rectangular and circular sections for the Euler-Bernoulli microbeam, they showed that by increasing the thickness or diameter to the size parameter of this frequency ratio decreases and equals one. Ke *et al*. (2012) investigated the nonlinear vibrations of Timoshinko's microbeam of FGM and obtained effects of the small-scale parameter on the natural frequency using the differential quadrature method. They showed that both of the linear and nonlinear frequencies increase significantly when the thickness of the FGM microbeam is comparable to the material length scale parameter. Rahmani *et al*. (2017) by using this theory, analysis of size-dependent bending and buckling of functionally graded microbeams with higher-order shear deformation beam model has been done. Al-Basyouni *et al*. (2015) using high-order theories such as sinusoidal theory, showed the effects of the material length scale parameter, the power law index, and shear deformation on the bending and dynamic behaviors of FG microbeams. Static and dynamic analysis of FGM micro-beam was performed using modified coupling stress theory (Ghayesh *et al*. 2017). They showed that the increase and decrease of the frequency in fag material depends on the power index coefficient. Ghayesh and Amabili (2014) studied the effects of small-scale parameter and amplitude of the initial imperfection on the coupled longitudinal-transverse behaviour of a geometrically imperfect microbeam. Using Galerkin method and pseudo-arclength technique, they showed that the increase These parameters increases the nonlinear natural frequency and also examined the effects of these parameters on the frequency response. Subsequently, the effects of nonlinear foundation on the frequency and force-response were investigated (Ghayesh and Farokhi 2015). It is known that when the microbeam with constant end supports are placed under transverse vibration, axial tension has been created, that nonlinearly it has been proportionate to transverse deflection of the beam and microbeam vibrates in the nonlinear mode. Şimşek (2014), uses the semi-analytic He's method to investigate the nonlinear nonlinear free vibration of the Euler-Bernoulli micro-beam on a nonlinear foundation. Ghayesh *et al*. (2013), used Galerkin method and arc-length to investigate forced vibration analysis of Euler-Bernoulli microbeam under dynamical forces using the modified couple stress theory and strain gradient. Kahrobaiyan *et al*. (2012) examined nonlinear static behaviour and free vibration of Euler-Bernoulli microbeam along with strain gradient theory and harmonic balance analysis method and compared it with modified couple stress theory. Nonlinear free size-dependent vibration behaviour in microbeams has been modified based on couple stress theory and has been investigated using Kantorovich and Shooting Method (Wang *et al*. 2013). In recent years, due to the applications of microbeam in intelligent systems, some studies have been conducted on nonlinear vibration under electrostatic tensile force and the important role of the length scale parameter on the hardening and softening has been investigated. Peng *et al*. (2017) performed a Dynamic analysis of size-dependent microbeams with nonlinear elasticity under electrical operation. They showed that a microbeam exhibiting nonlinear elastic stress-strain relationship has reduced effective stiffness while the size effect has the opposite effect. Jia *et al*. (2015) studied the combined effects of the size effect, material gradient, temperature change and electrical actuation on the microbeam Bernoulli-Euler by DQM. Viscoelastic effects play an important role in free and forced vibration of microbeam. Recent studies by Farokhi and Ghayesh (2017) show that with damping the increase of the damming parameter, the phenomenon of softening occurs and the modulus of elasticity decreases in microbeam reduces. Moreover, by increasing the small scale parameter hardening phenomenon occurs and there will be an increase in modulus of elasticity. The present study has examined free and forced vibrations analysis of nonlinear Euler-Bernoulli microbeams with different boundary conditions beased on orthotropic visco-Pasternak foundation. By using Newmark-beta method in each time step and differential quadrature method in each place step, the nonlinear to linear frequency ratio in free vibrations has been calculated. In the foundation, all the Winkler coefficients shear, nonlinear, orthotropic and damping coefficients are considered. Further, the temperature changes for materials whose temperature and mechanical properties are temperature dependent are investigated. Moreover, by changing the small-scale parameters, dynamic force range and all coefficients, deflection of microbeam in forced vibration has been investigated. The advantages of the proposed method are calculating the nonlinear frequency directly from the period of rotation, and contrary to many articles, it is not necessary to try and error to obtain nonlinear frequency from the linear frequency.

2. Governing equations

According to Euler-Bernoulli beam assumption that the vertical line to the neutral axis remains vertical after the deformation, the shear stresses are neglected. Therefore, the displacement field are expressed as follows

$$u_x(x,z,t)=u(x,t)-z\frac{\partial w(x,t)}{\partial x}\ ,\ u_z(x,z,t)=w(x,t) \tag{1}$$

(u,w) respectively, are longitudinal and transverse displacements at each point of the neutral axis. according to the assumption of small strain, the nonlinear strain-displacement relations are assumed in the following form

$$\begin{aligned}&\varepsilon_{xx}=\varepsilon_x^L+\varepsilon_x^{NL}\\&\varepsilon_{xx}=\frac{\partial u_x(x,z,t)}{\partial x}+\frac{1}{2}\left(\frac{\partial w(x,t)}{\partial x}\right)^2=\frac{\partial u(x,t)}{\partial x}-\\&\qquad z\frac{\partial^2 w(x,t)}{\partial x^2}+\frac{1}{2}\left(\frac{\partial w(x,t)}{\partial x}\right)^2\\&\varepsilon_{yy}=\varepsilon_{xy}=\varepsilon_{zz}=\varepsilon_{yz}=0\end{aligned} \tag{2}$$

In the above equation, ε_{xx} is the total longitudinal strain which equals to sum of the two components of linear strain ε_x^L and nonlinear strain ε_x^{NL} (resulting from high transverse deformation).

2.1 Modified couple stress theory

The strain energy of a system occupying region Ω, on the basis of the modified couple stress theory, can be formulated as (Park *et al*. 2016)

$$U_s=\frac{1}{2}\int_\Omega(\sigma:\varepsilon+m:\chi)dV \tag{3}$$

Where

$$\sigma=\lambda\, tr(\varepsilon)I+2\mu\varepsilon,\ \ \varepsilon=\frac{1}{2}\left[\nabla u+(\nabla u)^T\right] \tag{4}$$

$$m=2l^2\mu\chi,\qquad \chi=\frac{1}{2}\left[\nabla\theta+(\nabla\theta)^T\right] \tag{5}$$

σ is the symmetric part of stress tensor, $\boldsymbol{\varepsilon}$ is strain tensor, m is deviatoric part of the couple stress tensor and χ is symmetric part of the curvature tensor. λ and μ denote the Lam´e constants, **I** stand for the second-order identity tensor, and l represents the material length-scale parameter. The components of the infinitesimal rotation vector θ are related to the components of the displacement vector field u as

$$\theta=\frac{1}{2}curl\,u \tag{6}$$

When length scale parameter has been considered equal to zero, the above equations are converted into the governing equations for beams in the macro scale. Vector rotation component can be obtained using Eq. (6)

$$\theta_y=\frac{\partial w(x,t)}{\partial x},\qquad \theta_x=\theta_z=0 \tag{7}$$

By substituting Eq. (7) into Eq. (5), the curvature tensor can be expressed as

$$\chi_{xy}=\frac{1}{2}\frac{\partial^2 w(x,t)}{\partial x^2},\ \ \chi_{xx}=\chi_{yy}=\chi_{zz}=\chi_{xz}=\chi_{yz}=0 \tag{8}$$

3. Nonlinear governing equations

Hamilton's principle is used herein to derive the equations of motion. The principle can be stated in analytical form as (Reddy 2002)

$$\delta\int_0^t\left[K_e-(U_{\text{int}}-W_p-W_{ext})\right]dt=0 \tag{9}$$

Where δU *is the variation of strain energy*, δK_e is the variation of kinetic energy, δW_p is the variation of external force Caused by the effects of the orthotropic visco-Pasternak foundation and δW_{ext} is the variation of external force (Ghorbanpour-Arani and Shokravi 2013). As shown in Fig. 1, this microbeam is resting on the orthotropic visco-Pasternak foundation and L, A are the length and area of the micro-beam.

By putting Eqs. (4)-(5) into the Eq. (3), and the first variations of strain energy equation at the time interval [0, t] can be written

$$\begin{aligned}&\delta\int_0^t U_{\text{int}}dt=\int_0^t\int_\Omega\left(\sigma_{ij}\delta\varepsilon_{ij}+m_{ij}\delta\chi_{ij}\right)dVdt=\\&\int_0^t\int_0^L\left[N\left(\frac{\partial\delta u}{\partial x}+\frac{\partial w}{\partial x}\frac{\partial\delta w}{\partial x}\right)-\left(M+Y\right)\frac{\partial^2\delta w}{\partial x^2}\right]dxdt\end{aligned} \tag{10}$$

where (N, M) are the stress resultants and Y is couple moment defined as

$$(N,M,Y)=\int_A(\sigma_{xx},z\sigma_{xx},m_{xy})dA \tag{11}$$

The variation of potential energy of the applied loads can be expressed as

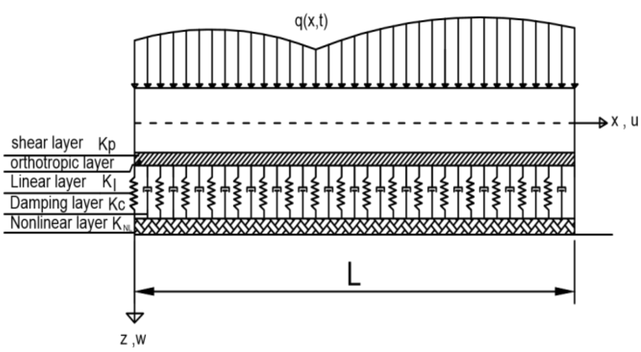

Fig. 1 Isotropic Euler-Bernoulli microbeam base on orthotropic visco-Pasternak foundation

$$\delta\int_0^t W_{ext}dt = \int_0^t\int_0^L \left(q\delta w + f\,\delta u\right)dxdt$$
$$\delta\int_0^t U_p dt = \int_0^t\int_0^L \begin{pmatrix} (k_L w + k_{Nl}w^3)\delta w - k_C w\dfrac{\partial \delta w}{\partial t} + \\ k_P\cos(\theta)\dfrac{\partial w}{\partial x}\dfrac{\partial \delta w}{\partial x}\end{pmatrix}dxdt \tag{12}$$

Where q is transverse distributed load f is axial load. k_L ,k_{NL} are, respectively, Winkler linear and nonlinear coefficients caused by vertical forces, k_C is foundation damping coefficient caused by viscosity effects and k_P is Pasternak coefficient caused by shear forces which changes under angle θ due to its orthotropic property. The first variations of kinetic energy in the time interval are equal to

$$\delta\int_0^t K_e\,dt = \int_0^t\int_0^L \rho A\left(\frac{\partial u}{\partial t}\frac{\partial \delta u}{\partial t} + \frac{\partial w}{\partial t}\frac{\partial \delta w}{\partial t}\right)dxdt \tag{13}$$

In the above equation ρ is the density of the microbeam.

By substituting Eqs. (11)-(13) into Eq. (9), we can obtain the following equations of motion

$$\delta u:\quad \frac{\partial N}{\partial x} + f = \rho A\frac{\partial^2 u}{\partial t^2} \tag{14}$$

$$\delta w:\quad \frac{\partial^2 M}{\partial x^2} + \frac{\partial^2 Y}{\partial x^2} + \frac{\partial}{\partial x}\left(N\frac{\partial w}{\partial x}\right) - k_L w - k_{NL}w^3 - k_C\frac{\partial w}{\partial t} + k_P\cos(\theta)\frac{\partial^2 w}{\partial x^2} + q = \rho A\frac{\partial^2 w}{\partial t^2} \tag{15}$$

3.1 Effects of temperature change

In this section, we study the effects of temperature variations, whose mechanical and thermal properties are temperature-dependent. The mechanical and thermal properties of the microbeam are as follows (Farokhi and Ghayesh 2015)

$$\begin{aligned}&\alpha(T) = [3.725(1-\exp(-5.88\times10^{-3}(T-124))) + 5.548\times10^{-4}T]10^{-6}\ (K^{-1})\\ &E(T) = E_0[1-74.87\times10^{-6}(T-T_0) - 45.14\times10^{-9}(T-T_0)^2];\ E_0 = 165.46Gpa\\ &\mu(T) = \mu_0[1-60.16\times10^{-6}(T-T_0) - 51.28\times10^{-9}(T-T_0)^2];\ \mu_0 = 165.46Gpa\end{aligned} \tag{16}$$

The E_0 and μ_0 are Young's modulus, and shear modulus at the initial temperature of the room and α is the expansion coefficient. N^T, M^T are the stress resultants from change temperature defined as

$$(N^T, M^T) = -\int_A E(T).\alpha(T).\Delta T(1,z)dA \tag{17}$$

Where ΔT is the uniform temperature rise in the microbeam. To simplify further analysis, the equations of motion are dimensionless by defining

$$\zeta = \frac{x}{L}\ ,\tau = \frac{t}{L}\sqrt{\frac{E}{\rho}}\ ,U = \frac{u}{L}\ ,W = \frac{w}{L}\ , f^* = \frac{Lf}{EA}\ ,$$
$$r = \frac{1}{L}\sqrt{\frac{I}{A}} = R/L\ ,\eta = \frac{l}{L}\ ,q^* = \frac{Lq}{EA},\ K_L = \frac{k_L L^2}{EA}\ ,$$
$$K_C = \frac{k_C}{A}\sqrt{\frac{1}{\rho E}}\ ,K_{NL} = \frac{k_{NL}L^4}{EA}\ ,K_P = \frac{k_P}{EA} \tag{18}$$

In the above equations, the value of $R = \sqrt{I/A}$ is the radius of gyration for the cross-section of microbeam and $r = R/L$ is expressed as dimensionless radius of gyration and for rectangle cross-section equal to $r = (1/2\sqrt{3})h/L$ Which represents the ratio of thickness to length. By putting the dimensionless parameters and Eqs. (16)-(17) into Eqs. (14)-(15) can be rewritten as dimensionless equations of motion

$$\frac{\partial^2 U}{\partial \tau^2} - \frac{\partial^2 U}{\partial \zeta^2} - \frac{\partial W}{\partial \zeta}\frac{\partial^2 W}{\partial \zeta^2} = f^* \tag{19}$$

$$\frac{\partial^2 W}{\partial \tau^2} + \left[r^2 + \frac{\eta^2}{2(1+\upsilon)}\right]\frac{\partial^4 W}{\partial \zeta^4} - \frac{\partial U}{\partial \zeta}\frac{\partial^2 W}{\partial \zeta^2} - \frac{\partial^2 U}{\partial \zeta^2}\frac{\partial W}{\partial \zeta} - \frac{3}{2}\left(\frac{\partial W}{\partial \zeta}\right)^2\frac{\partial^2 W}{\partial \zeta^2} + \alpha.\Delta T\frac{\partial^2 W}{\partial \zeta^2} + K_L W + K_{NL}W^3 + K_C\frac{\partial W}{\partial \tau} - K_P\cos(\theta)\frac{\partial^2 W}{\partial \zeta^2} = q^* \tag{20}$$

Using the remaining terms of the integral in the Eq. (9), Boundary conditions are obtained, and for the different boundary conditions are given in Table 3 of Appendix B.

4. Solution of the problem

To solve the nonlinear governing Eqs. (19) and (20), which include partial differential equations, the DQ method for space function according to Appendix A is used and is used by the Newmark-beta method to function in the time domain. Substitution of Eq. (35) into Eqs. (19) and (20) for linear terms and Eq. (39) into Eqs. (19) and (20) for nonlinear terms yields the following expression

$$[I]\{\ddot{U}\} - [B]\{U\} - [a_1][B]\{W\} = \{f^*\} \tag{21}$$

$$[I]\{\ddot{W}\} - K_C[I]\{\dot{W}\} + a[D]\{W\} - [a_2][A]\{U\} - [a_3][B]\{U\} - \frac{3}{2}[a_4][B]\{W\} - [\alpha.\Delta T][B]\{W\} - K_L[I]\{W\} - K_{NL}[a_5][I]\{W\} + K_P\cos(\theta)[B]\{W\} = \{q^*\} \tag{22}$$

Where, a_i are coefficients of the Eqs. (19) and (20). The Eqs. (21)-(22) can be written in matrix and compact form as

$$\begin{bmatrix} I & [0] \\ [0] & I\end{bmatrix}\begin{Bmatrix}\ddot{U}\\ \ddot{W}\end{Bmatrix} + \begin{bmatrix}[0] & [0]\\ [0] & -K_C I\end{bmatrix}\begin{Bmatrix}\dot{U}\\ \dot{W}\end{Bmatrix} + \begin{bmatrix}[-B] & [-a_1 B]\\ [a_2 A - a_3 B] & \begin{bmatrix} aD - \frac{3}{2}a_4 B - \alpha\Delta T B - K_L I \\ + K_P\cos(\theta)B - K_{NL}a_5 I\end{bmatrix}\end{bmatrix}\begin{Bmatrix}U\\ W\end{Bmatrix} = \begin{Bmatrix}f^*\\ q^*\end{Bmatrix} \tag{23}$$

If the longitudinal and transverse displacements are described as an overall displacement $\{V\}$, and vector coefficients $\{W\}$ have been factored out, Eq. (23) can be rewritten

$$[M]\{\ddot{V}\}+[C]\{\dot{V}\}+([K_L]+[K_{NL}](W))\{V\}=\{\bar{F}\} \tag{24}$$

In the above equation $[M]$ is mass identity matrix and $[C]$ is damping matrix and $[K]$ is stiffness matrix which composed of two linear and nonlinear parts. Eq. (24) has been nonlinear eigenvalues problem and its solution can be done by application of iterative calculations (Zhong and Guo 2003). Typically, at first, the nonlinear term is considered equal to zero (K_{NL}) and the resulting eigenvalues problem is solved. Values and linear eigenvectors (stiffness and system linear frequency) are achieved, and then the linear terms are placed in the overall equation to obtain the nonlinear term. The eigenvalues problem is solved again in order to obtain linear eigenvectors and eigenvalues again (stiffness and system nonlinear frequency). In the nonlinear analysis of eigenvalues problem, system stiffness matrix is a function of eigenvector and this makes computing eigenvalues (natural frequencies) more difficult. This problem complicates the calculation of frequencies since every multiple of an eigenvector is an eigenvector itself. In addition, this method ignores the effects of initial conditions problem in nonlinear vibrations. To solve this problem in this paper the following method will be used:

Step one: When external forces is equal to zero, the system under initial conditions of displacement and without the initial velocity will be moved. The intended displacement at the initial time will perfectly match hypothetical mode shape of a system.

Step two: Using the Newmark-beta method at each time step, beam response will be obtained. This issue will be dully explained in Section 5.

Step three: Considering obtained free oscillations, the arc-length method can be used to obtain the period for free vibration mode.

Step four: Nonlinear natural frequency can be obtained from ($\omega = 2\pi/T_f$).

Step five: Using differential quadrature method in Appendix A, spatial solution is offered and frequency ratio can be calculated.

Fortunately for the calculation of the period and the nonlinear natural frequency, examining response time over a period of oscillation is enough. Since in nonlinear mode by increasing the initial amplitude, the period decreases, therefore, in all analyses, examining response in period which is equivalent to a period in linear mode is sufficient.

5. Newmark beta method

Newmark method is a numerical method for solving differential equations of two order, in which is the acceleration variations can be approximated in sequential time intervals. According to partial differential Eq. (24), with the help of Newmark method this partial differential equation which is in terms of time and place can be defined in terms of place at certain time steps and then can be solved using differential quadrature method. Consider stiffness $[K]$, mass $[M]$, damping $[C]$ and the force vector ($[F(t)]$) matrices. Then the initial conditions are applied into the equation, i.e., $\{X_0\}$, $\{\dot{X}_0\}$ and $\{\ddot{X}_0\}$ which respectively represent the change of initial position, initial velocity, and initial acceleration of midpoint of microbeam (Newmark 1959). By applying the initial conditions of the problem, general form of Eq. (24) is expressed as follows

$$\{\ddot{X}_0\}=[M(0)]^{-1}\left(\{F(0)\}-[C(0)]\{\dot{X}_0\}-[K(0)]\{X_0\}\right) \tag{25}$$

Determining the appropriate value for α and β in the time step Δt, and calculating the following coefficients play an important role in the convergence of problem.

$$\begin{gathered} a_0=\frac{1}{\beta(\Delta t)^2} \quad a_1=\frac{\alpha}{\beta\Delta t} \quad a_2=\frac{1}{\beta\Delta t} \\ a_3=\frac{1}{2\beta}-1 \quad a_4=\frac{\alpha}{\beta}-1 \quad a_5=\frac{\Delta t}{2}\left(\frac{\alpha}{\beta}-2\right) \end{gathered} \tag{26}$$

It should be noted that usually the following values for convergence are suggested

$$\alpha=\frac{1}{2} \quad \frac{1}{6}\le\beta\le\frac{1}{4} \tag{27}$$

For stability of solutions, observing the following condition for time step Δt for solving time T_f is necessary

$$\frac{\Delta t}{T_f}\le\frac{1}{\pi\sqrt{2}}\frac{1}{\sqrt{\alpha-2\beta}} \tag{28}$$

For β = 1/4, for stability of solutions, time intervals should be equal to $(\Delta t/T_f) \le \infty$, and for β = 1/6, is equal to $(\Delta t/T_f) \le (\sqrt{3}/\pi)$. The effective stiffness matrix is defined as follows

$$[\bar{K}]=[K]+a_0[M]+a_1[C] \tag{29}$$

For each time step, effective force vector is recommended based on its values at previous time of the following algorithm:

Step A: Using Eq. (23) can be written

$$\begin{aligned} \{\bar{F}_{t+\Delta t}\}=\{F_{t+\Delta t}\}&+[M]\left(a_0\{X_t\}+a_2\{\dot{X}_t\}+a_3\{\ddot{X}_t\}\right) \\ &+[C]\left(a_1\{X_t\}+a_4\{\dot{X}_t\}+a_5\{\ddot{X}_t\}\right) \end{aligned} \tag{30}$$

Step B: Using the following equation, displacement vector at the time $t+\Delta t$ is calculated

$$\{X_{t+\Delta t}\}=[\bar{K}]^{-1}\{\bar{F}_{t+\Delta t}\} \tag{31}$$

Step C: Using the following equations, the velocity and acceleration at the time $t+\Delta t$ are calculated

$$\begin{aligned} \{\dot{X}_{t+\Delta t}\}&=a_1\left(\{X_{t+\Delta t}\}-\{X_t\}\right)-a_4\{\dot{X}_t\}-a_5\{\ddot{X}_t\} \\ \{\ddot{X}_{t+\Delta t}\}&=a_0\left(\{X_{t+\Delta t}\}-\{X_t\}\right)-a_2\{\dot{X}_t\}-a_3\{\ddot{X}_t\} \end{aligned} \tag{32}$$

Step D: With returning to the step A of the problem, the same steps are carried out for the next time step to converge the problem

6. Numerical results

In these examples, we characterize nonlinear natural frequency and response frequency of microbeam rest on nonlinear orthotropic visco-Pasternak foundation with temperature change. Our studies have been carried out in three stages, which include free vibration, compulsory and temperature changes. At first, the temperature changes are ignored and only the effects of the foundation coefficients have been investigated, but in the end, the effects of temperature variations on materials whose mechanical and thermal properties are temperature dependent are investigated.

6.1 Example 1

For numerical illustrations of mechanical properties of microbeam, with different boundary conditions is herein considered Rao (2007)

$$[r = 0.029; v = 0.25;\ \eta = 0; \Delta T = 0]$$

In this example, the nonlinear free vibration frequencies were calculated. For validation and comparison with Article Rao (2007), length scale parameter and damping coefficient of foundation length scale parameter are considered zero. As it is clear, the nonlinear natural frequency has been obtained with good accuracy according to Table 1. Then, by changing the parameter radius of gyration (r) for different support conditions, the nonlinear natural frequency is calculated. It should be noted that according to the type of dimensionless time in Eq. (18) and using equation ($\lambda\tau = \Omega\, t$), is obtained dimensional frequency. The value of Ω is the dimensional frequency and λ is dimensionless frequency. In reference Rao (2007) the relationship of dimensionless frequency Ω with the dimensional frequency λ is as follow

$$\Omega = \sqrt{\frac{\lambda}{r}} \tag{33}$$

Table 1 Comparison of the nonlinear frequency for various boundary conditions

N^*	C_C	C_S	S_S	C_F
	Ω_{NL}^*	Ω_{NL}^*	Ω_{NL}^*	Ω_{NL}^*
7	4.756793	3.954783	3.151371	1.875362
8	4.749756	3.946545	3.151478	1.875247
9	4.749938	3.946447	3.151539	1.875109
10	4.750046	3.946598	3.151592	1.875103
11	4.750043	3.946605	3.151593	1.875104
12	4.750041	3.946602	3.151593	1.875104
Rao (2007)	4.749779	3.930137	3.149049	1.867153

* Ω_{NL}: Nonlinear frequencies; *N: Number of nodes

In Table 1, nonlinear natural frequencies converge to 12 points.

As the Table 1 shows, the nonlinear frequency obtained in this article is greater than the frequency provided in the article (Rao 2007). This is Due to more nonlinear terms than Rao’s article in governing equations which represents more hardening in the system. Now the effect of dimensionless parameter r (radius of gyration) on nonlinear frequency of the transverse vibrations is examined and here the small scale parameter is η = 0.1. The ratio of length to thickness and small scale parameter to thickness are L/h = 10 and l/h = 1, As a result, the ratio small scale parameter to length is equal to ($\eta = l/L$ 0.1).

As the radius of gyration increases, the nonlinear frequency increases, and because of increasing the radius of gyration, the thickness of the microbeam increases with respect to its length. With the thickening and shortening of the microbeam, the natural frequency increases (Figs. 2-4). In other words, an increase in the radius of gyration caused hardening in the system and an increase in Poisson coefficient results in softening. Now, the effects of different

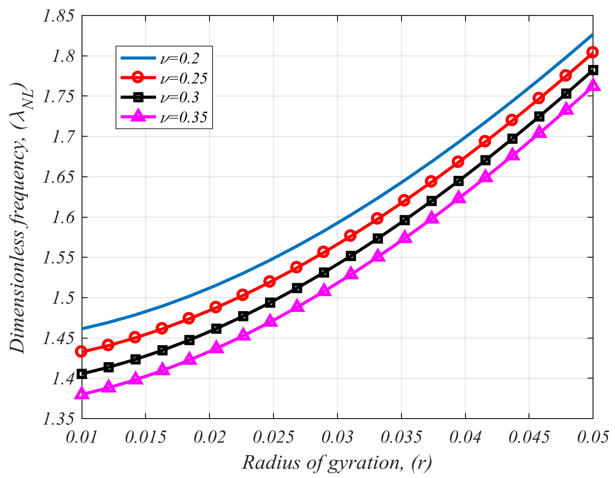

Fig. 2 The effect of radius of gyration and Poisson’s ratio on the dimensionless frequency (C_C)

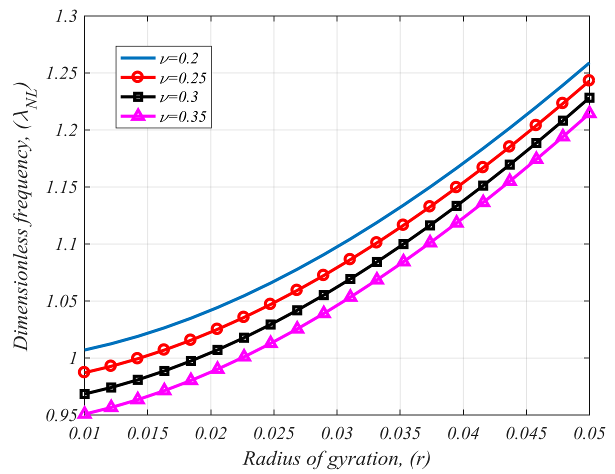

Fig. 3 The effect of radius of gyration and Poisson’s ratio on the dimensionless frequency (C_S, non-sliding)

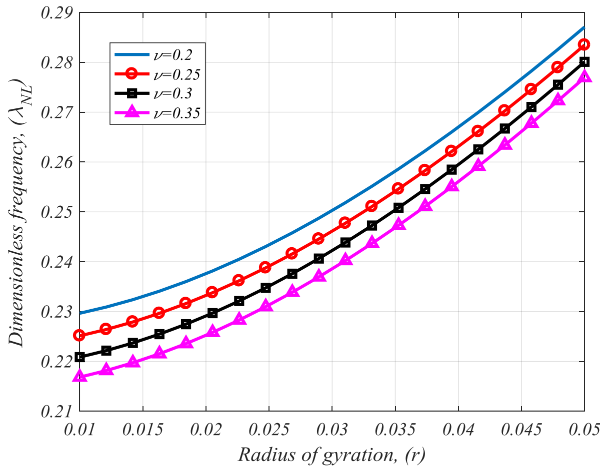

Fig. 4 The effect of radius of gyration and Poisson's ratio on the dimensionless frequency (C_F)

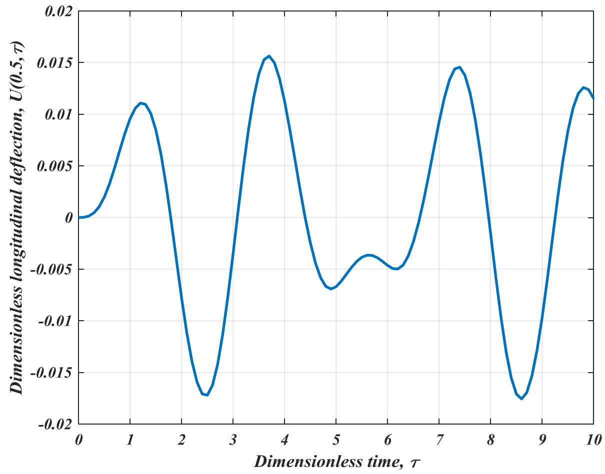

Fig. 6 Time response of beam in forced longitudinal vibration under dynamic load (C_C)

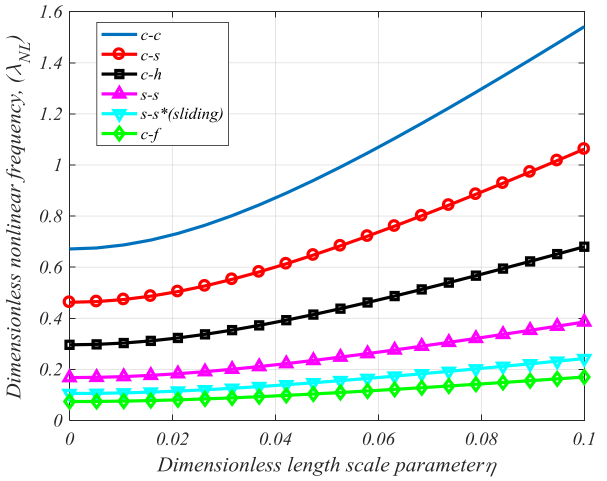

Fig. 5 The effect of length scale parameters under different boundary conditions on nonlinear natural frequencies

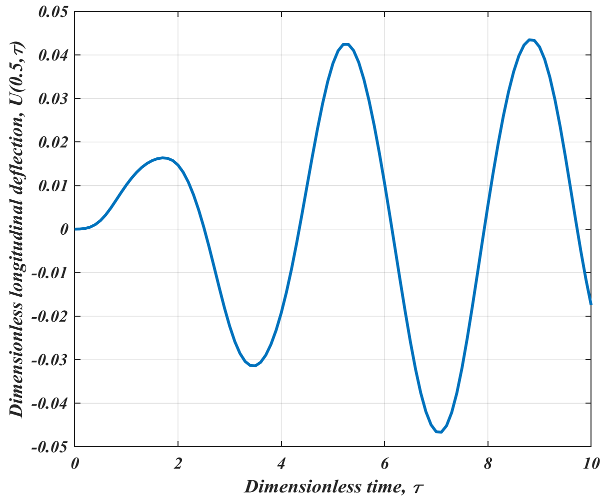

Fig. 7 Time response of beam in forced longitudinal vibration under dynamic load (C_F)

boundary conditions and the length scale parameter on the nonlinear natural frequency are investigated**.**

It has been shown that increasing length scale parameter results in an increase in all frequencies and this change reflects the beam stiffness increase by increasing this parameter. Moreover, as shown in the charts, as we move on from constrained support conditions like (C_C) to freer conditions of constrains such as (C_F), the nonlinear natural frequency reduces.

6.1.1 Forced vibration

To evaluate the effect of boundary conditions on the dynamic response of the beam in the longitudinal direction, assume a beam under dimensionless longitudinal load $f^*=0.1(1-\zeta)\sin(2\tau)$ and non-damping zero initial conditions. In Figs. 6-7, the variations of midpoint of the beam (ζ = 0.5) in both cases of boundary conditions are shown. As shown in these figures, in the case where both ends of the beam are constrained in the longitudinal direction (C_C), the oscillation amplitude will be less compared to (C_F) beam. In other words, as the constraints increases the natural frequency and decreases the range of motion in forced vibrations.

In order to evaluate the effect of thickness to beam length ratio on the beam dynamic response in transverse vibrations, a two-hinged beam with υ = 0.3 and η = 0.1 specifications under dimensionless transverse load $q^*=0.01exp(-0.1\tau)\sin(\pi\zeta)$ and zero initial conditions has been considered. In this case, all the coefficients of the foundation other than the damping coefficient is considered zero (K_C = 0.0001). Fig. 8 shows the changes in displacement time of midpoint of the beam in terms of time in different values of r. This figure indicates that by increasing the thickness to beam length ratio, the oscillation amplitude decreases.

In order to evaluate the effect of length scale parameter on the beam dynamic response in transverse vibrations, a beam (C_F) with υ = 0.3 and r = 0.03 specifications under dimensionless transverse load q^* = $0.005\zeta^2\sin(0.5\tau)$ and zero initial conditions should be taken into account. Fig. 9 shows changes in displacement time of the beam's end

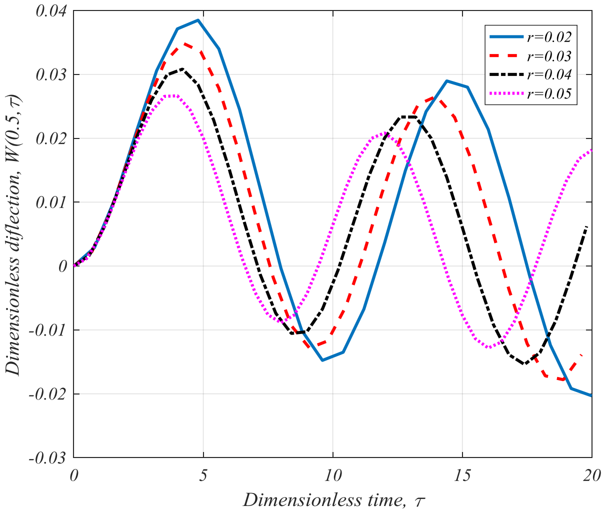

Fig. 8 Time response of beam in forced transverse vibration for different values of gyration radius

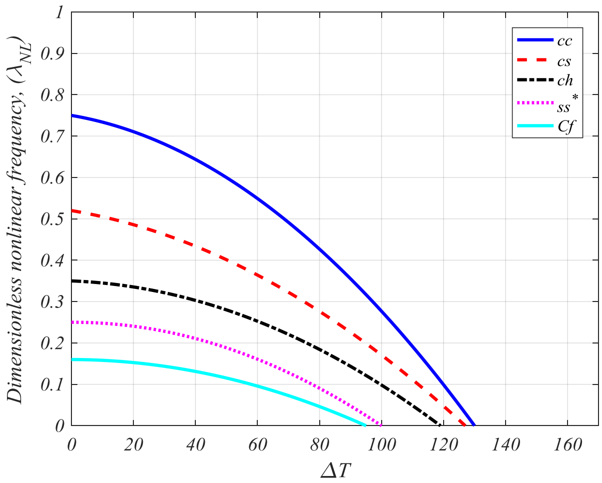

Fig. 10 The effect of temperature changes on the natural frequency with different boundary condition

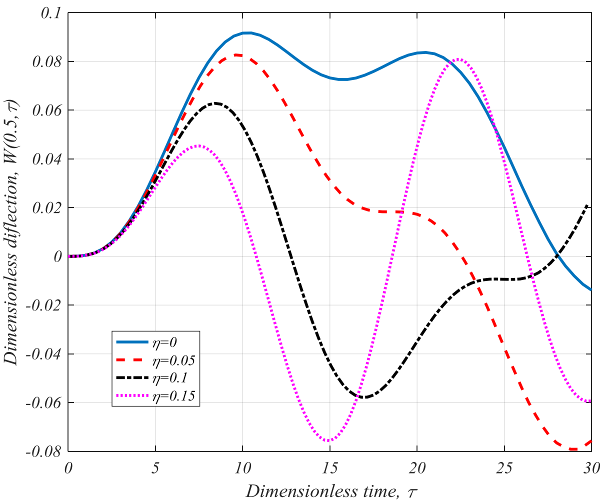

Fig. 9 Time response of beam in forced transverse vibration for different values of small scale parameter. (C_F)

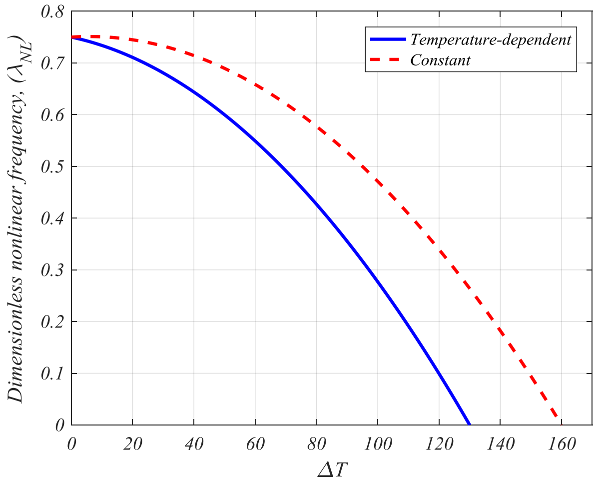

Fig. 11 The effect of temperature changes on the natural frequency

point in terms of time for different values of η. As this diagram shows, as the small scale parameter and the stiffness of the beam increase, the beam oscillation amplitude decreases.

6.1.2 changed temperature

Using Eqs. (19) and (2), the effects of temperature variations on nonlinear frequency are investigated. The relevant material properties for temperature dependent material considered are as follows

$$[r = 0.029;\ \ \eta = 0.1;\ \Delta T = 0\ to\ 250(K)]$$
$$\mu(T) = \frac{E(T)}{2\big(1 + v(T)\big)};$$

In Fig. 10, the nonlinear natural frequency decreases with increasing temperature. As it is known, the more restrictive the boundary conditions, the more expensive the system will be and the frequency will decrease later than the temperature change. This is the frequency reduction in the pre-buckling area, but the behavior of the system changes during post-buckling phenomenon. In Fig. 11, the micro-beam is temperature dependent and independent of temperature. The nonlinear natural frequency for temperature dependent materials decreases with increasing temperature. As a result, the buckling phenomenon in these materials is faster and changes in the temperature of about ΔT = 120. The results are good overlap with Farokhi and Ghayesh (2015).

6.2 Example 2

In this example, according to the paper Şimşek (2014), a micro-beam under free and compulsive vibration, and finally, the effects of temperature changes, are analysed and validation. In order for the dimensionless parameters mentioned in this article be the same with the mentioned reference, the following values for these variables and coefficients and initial conditions have been suggested

$$K_L = .04;\ K_P = .08,;\ K_{NL} = 10;\ \theta = 0;\ K_C = 0;$$
$$r = 0.029;\ \eta = \frac{l}{L} = (0, 0.025, 0.05, 0.075, 0.1) \tag{34}$$

Initially, the value L/h = 10 is chosen. As the ratio of the length to thickness parameter changes in the Şimşek (2014), between zero and one, the η ratio in this article varies from zero to 0.1. In two cases of (S_S) and (C_C) which have been evaluated in the following table, the value of dimensionless amplitude (X_0) = W_{max}/r is defined to achieve validation.

In Table 2, by N = 11 nods and time step Δt = 0.01, the converges and the final obtained answer nicely to the papers (Azrar *et al*. 1999, Şimşek 2014). As shown in the table above, the ratio of the frequencies obtained in this paper is greater than Azrar *et al*. (1999), and less than Şimşek (2014). In the first paper, linearization has been done and less nonlinear terms have been considered, but in the second paper, the semi-analytic method has been used. With more nonlinear terms, the stiffness of the system increases and nonlinear frequencies increase. These two papers can be used for C-C and S-S boundary conditions, but the method presented in this paper is applicable to any boundary condition.

Table 2 Comparison of the nonlinear frequency ratios obtained for various values of dimensionless amplitude for CC and SS

Dimensionless amplitude	C_C	C_C	C_C	S_S	S_S	S_S
X_0	Present	Simsek (2014)	Azrar *et al.* (1999)	Present	Simsek (2014)	Azrar *et al.* (1999)
1	1.0225	1.0231	1.0221	1.0893	1.0897	1.0891
2	1.0864	1.0897	1.0856	1.3219	1.3228	1.3177
3	1.1913	1.1924	1.1831	1.6381	1.6393	1.6256
4	1.3194	1.3228	1.3064	1.9840	2.000	-

The reason for this is that unlike the linear mode in which natural frequencies are only a function of the geometry of the system, in nonlinear natural frequencies, in addition to the geometry of the system, it also depends on initial conditions. In order to show this issue, an (S_S) beam with regard to initial conditions $W(\zeta, 0) = W_{max}\sin(\pi\zeta)$ is considered. In addition, for (C_C) beam, $W(\zeta, 0) = W_{max}/2[1-\cos(2\pi\zeta)]$ which exactly matches the first microbeam mode, has been taken into account. Then by assuming the other parameters to be constant and taking into account damping coefficient K_C = .0008, the variations of foundation coefficients on the frequency ratio has been investigated. Fig. 12(a) is related to the two ends of simple support (S-S) and Fig. 12(b) is related to the two ends of the clamp support (C-C) for all the following figures.

By assuming all coefficients and changes of Winkler coefficient to be constant, as it is shown in Figs. 13(a)-(b), as this coefficient increases, the frequency ratio decreases. As it is specified, the frequency ratio for (S-S) mode is greater; however, its reduction compared to (C-C) mode is greater. This shows that by increasing the constraints, the system stiffness increases and the frequency ratio decreases. Variations of frequency ratio for length scale parameter are the same' i.e., as the length scale parameter increases, the frequency ratio decreases.

In Figs. 12(a)-(b), by assuming Winkler coefficient (K_L = 0.08) to be constant, the Pasternak coefficient on the frequency ratios has been evaluated. As specified in Figs. 12(a)-(b), by increasing Pasternak coefficients and length scale parameter, the frequency ratio reduces. According to orthotropic property of the foundation, Pasternak coefficient which is caused by shear stresses depends on the shear angle. For this reason, Figs. 14(a)-(b) has examined this coefficient and its effects of its changes that and as it is observed as the shear angle increases, in contrast to the previous modes, the frequency ratio increases. The increase of the frequency ratio for (S_S) mode by changing the shear angle is greater than (C_C) mode and it shows that when the angle increases, as the body is more constrained, the frequency rate is less. In the following, nonlinear coefficient on the frequency ratio will be discussed. In this case, as

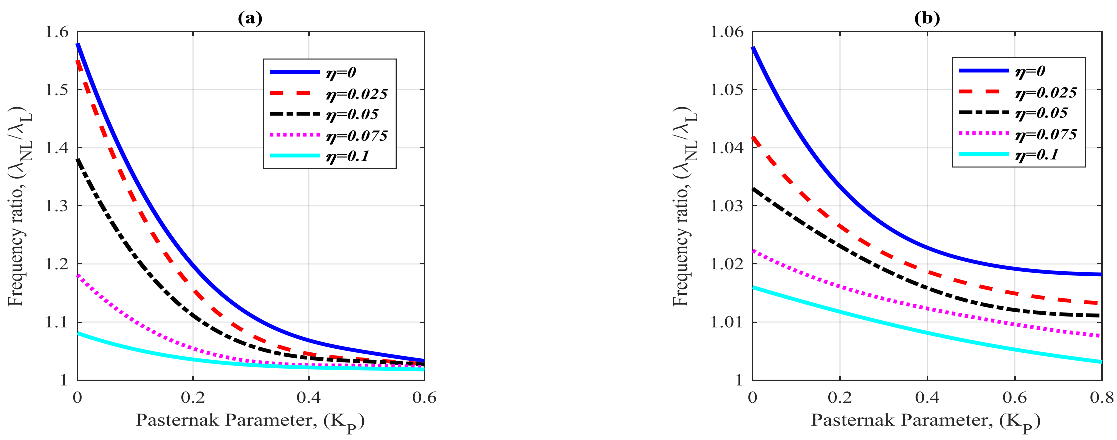

(a) Simple_simple (b) Clamp_clamp

Fig. 12 Variation of the nonlinear frequency ratio with the Pasternak parameter (shear parameter) for various values of the dimensionless length scale parameter

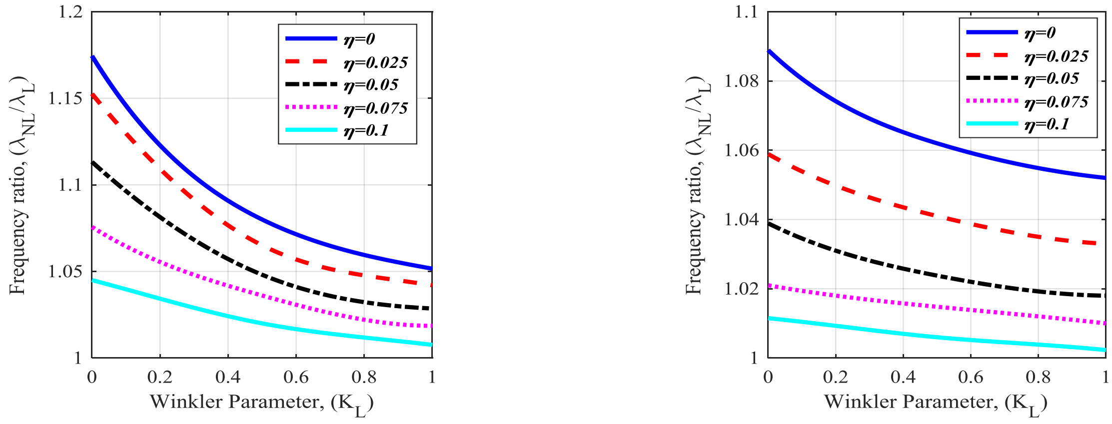

(a) Simple_simple (b) Clamp_clamp

Fig. 13 Variation of the nonlinear frequency ratio with the Winkler parameter for various values of the dimensionless length scale parameter

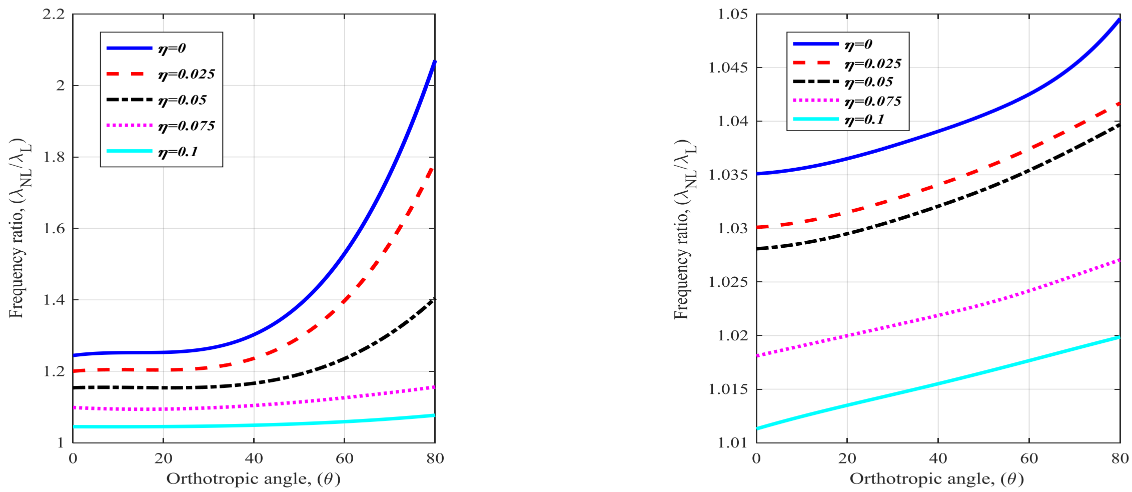

(a) Simple_simple (b) Clamp_clamp

Fig. 14 Variation of the nonlinear frequency ratio with the Orthotropic angle parameter for various values of the dimensionless length scale parameter

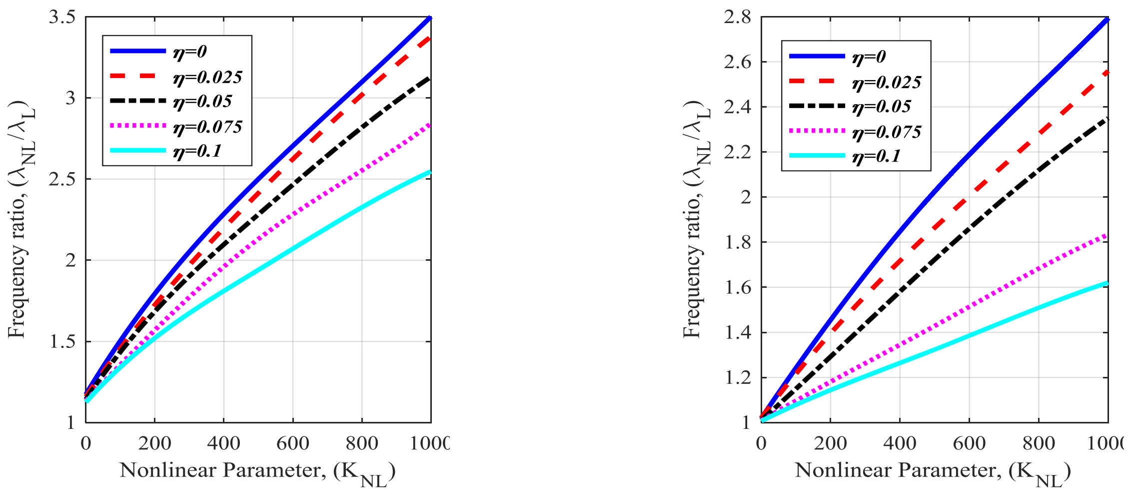

(a) Simple_simple (b) Clamp_clamp

Fig. 15 Variation of the nonlinear frequency ratio with the nonlinear parameter for various values of the dimensionless length scale parameter

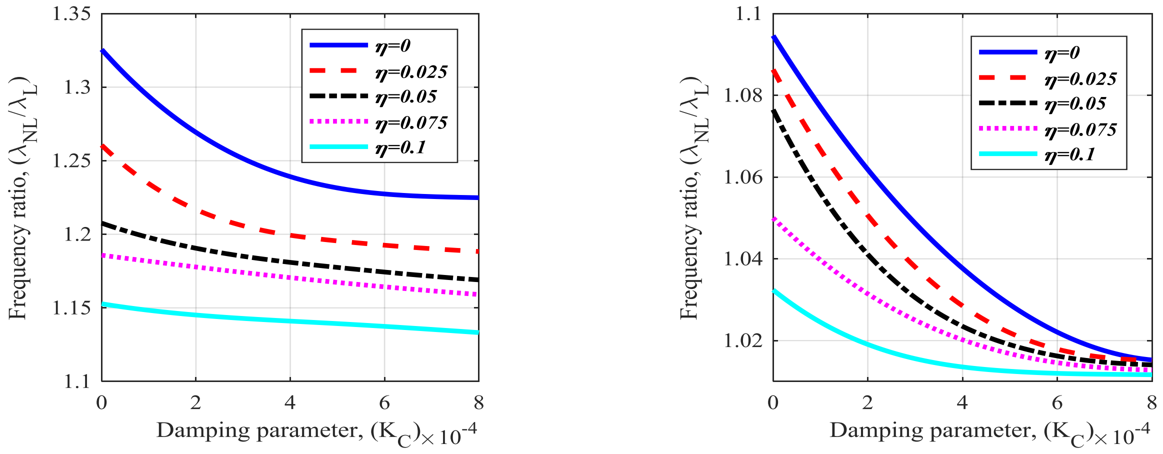

(a) Simple_simple (b) Clamp_clamp

Fig. 16 Variation of the nonlinear frequency ratio with the Damping parameter for various values of the dimensionless length scale parameter

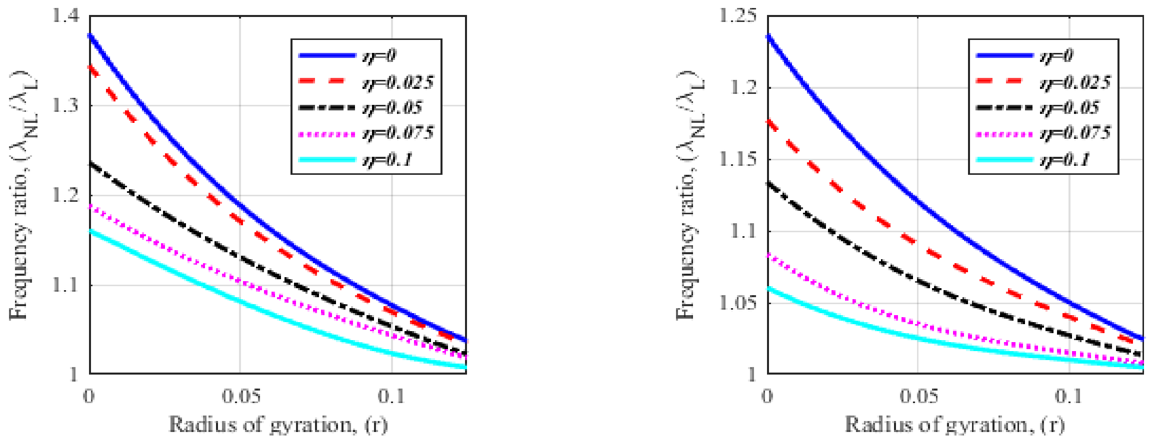

(a) Simple_simple (b) Clamp_clamp

Fig. 17 Variation of the nonlinear frequency ratio with the dimensionless radius of gyration parameter for various values of the dimensionless length scale parameter

shown in Figs. 15(a)-(b), as the nonlinear coefficient increases, frequency ratio increases and unlike the two Winkler and Pasternak coefficients, it is in foundation. It also shows the importance of evaluation of nonlinear mode in the foundation. Figs. 16(a)-(b) shows that as the damping coefficient increases, frequency ratio decreases. Moreover, the effects of gyration radius on the frequency ratio have been investigated for a micobeam with rectangular cross section. This coefficient is directly proportional to the thickness. As it is specified in Figs. 17(a)-(b), as the radius of gyration increases, frequency ratio decreases. This is due to an increase in the thickness of the beam and an increase in the stiffness of the system. As the radius of gyration increases, the frequency ratio converges towards one and whatever the radius is less, the frequency ratio is greater. This shows that evaluation of nonlinear mode for thin-walled and small beams is very important. Initial conditions W_{max} play an important role on the frequency ratio. As Figs. 18(a)-(b), suggests, as this coefficient increases, the frequency ratio increases. The same evaluation has been performed in Figs. 19(a)-(b) on beam midpoint displacement and it is observed that when the damping coefficient is zero, the range of motion is harmonic and with no decrease over time. However, by increasing the damping coefficient, amplitude of oscillation reduces and system becomes damped. The comparison of these two graphs perfectly confirms that in linear mode, natural frequency (vibration's period) is completely independent of the initial conditions. However, in nonlinear mode, an increase in amplitude in the initial conditions decreases the oscillation period. In other words, the natural frequencies increase.

6.2.1 Forced vibration analysis

In this section, regardless of longitudinal load ($f^* = 0$), microbeam forced vibration under dynamic force $q^* = q_0 exp(-0.1\tau)\sin(\pi\xi)$ has been investigated. An increase in the amplitude of the applied force, the beam oscillations amplitude will also increase that it is quite obvious. Another thing that can be concluded is that in all modes, oscillations amplitude in less nonlinear mode has been less than the

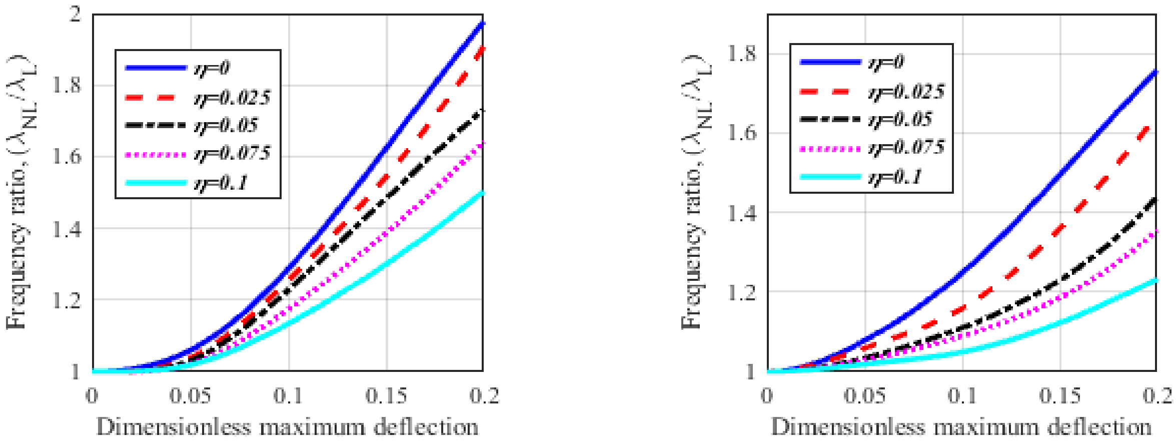

(a) Simple_simple (b) Clamp_clamp

Fig. 18 Variation of the nonlinear frequency ratio with the dimensionless of maximum deflection parameter for various values of the dimensionless length scale parameter

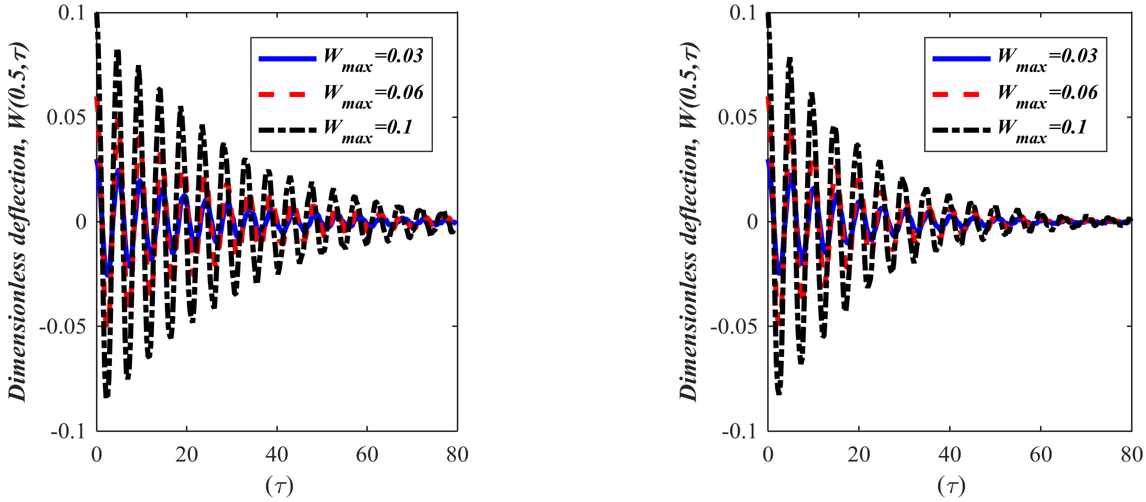

(a) Simple_simple (b) Clamp_clamp

Fig. 19 Variation of the dimensionless midpoint displacement with the dimensionless time for K_c = .08 and for various values of the maximum deflection

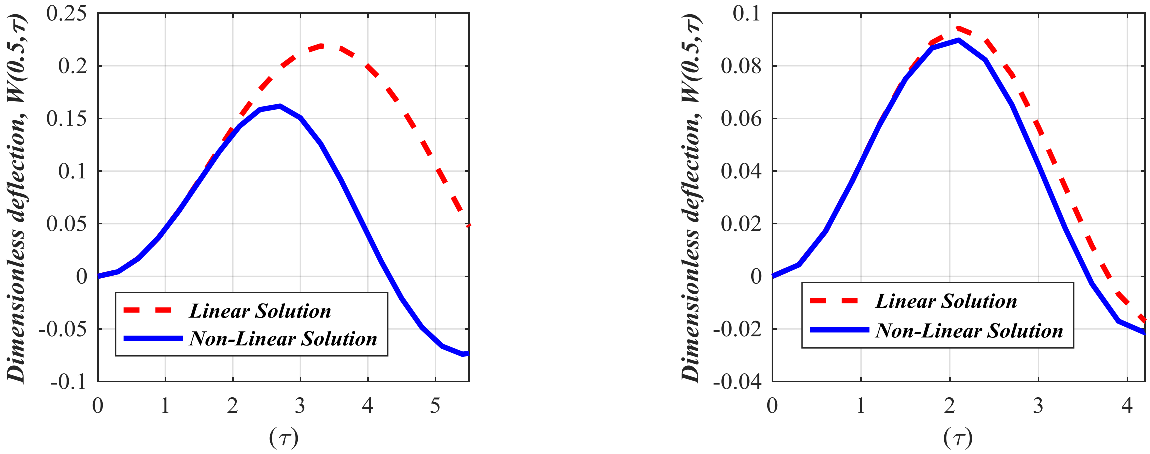

(a) Simple_simple (b) Clamp_clamp

Fig. 20 Variation of the dimensionless midpoint displacement with the dimensionless time for q_0 = 0.1, η = .075 and for linear and nonlinear microbeam.

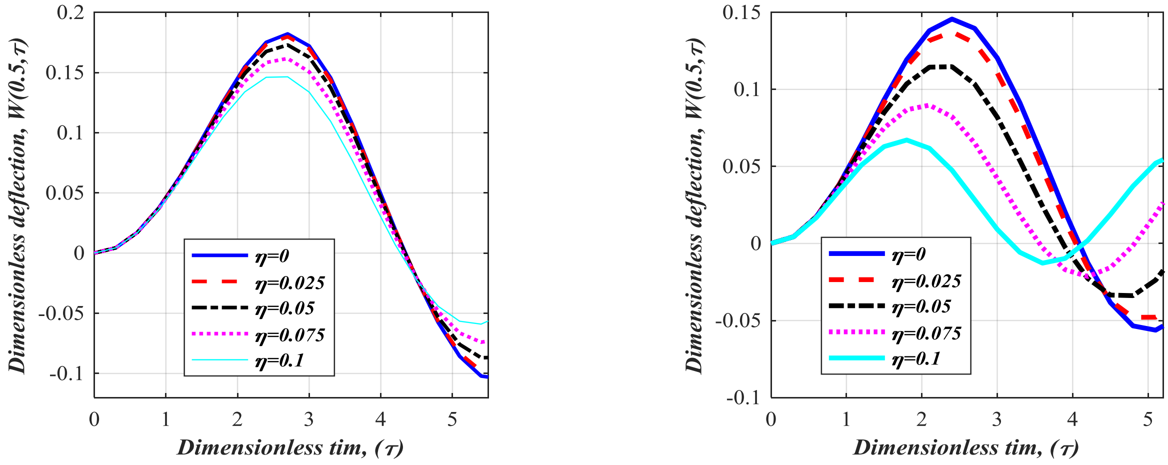

(a) Simple_simple (b) Clamp_clamp

Fig. 21 Variation of the dimensionless midpoint displacement with the dimensionless time for q_0 = 0.1, and for various values of the length scale parameters

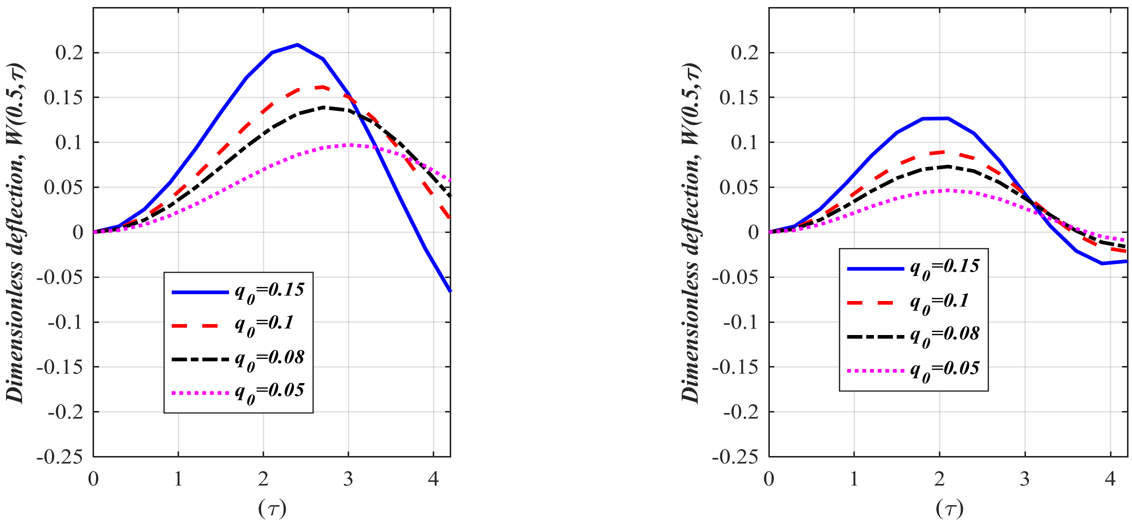

(a) q_0 = 0.1, simple_simple (b) q_0 = 0.1, clamp_clamp

Fig. 22 Variation of the dimensionless midpoint displacement with the dimensionless time for η = 0.075, and for various values of the amplitude force

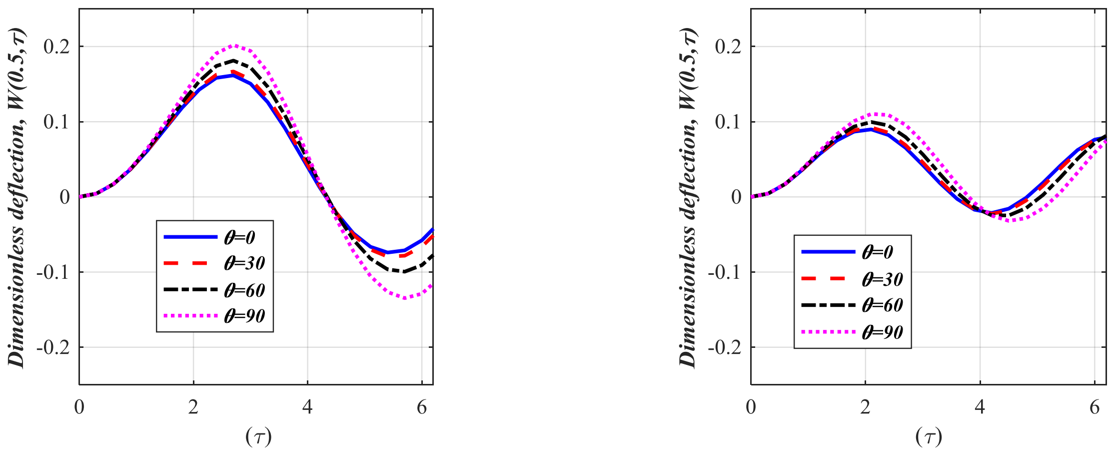

(a) η = 0.075, simple_simple (b) η = 0.075, clamp_clamp

Fig. 23 Variation of the dimensionless midpoint displacement with the dimensionless time for η = 0.075, and for various values of the angles of orthotropic foundation

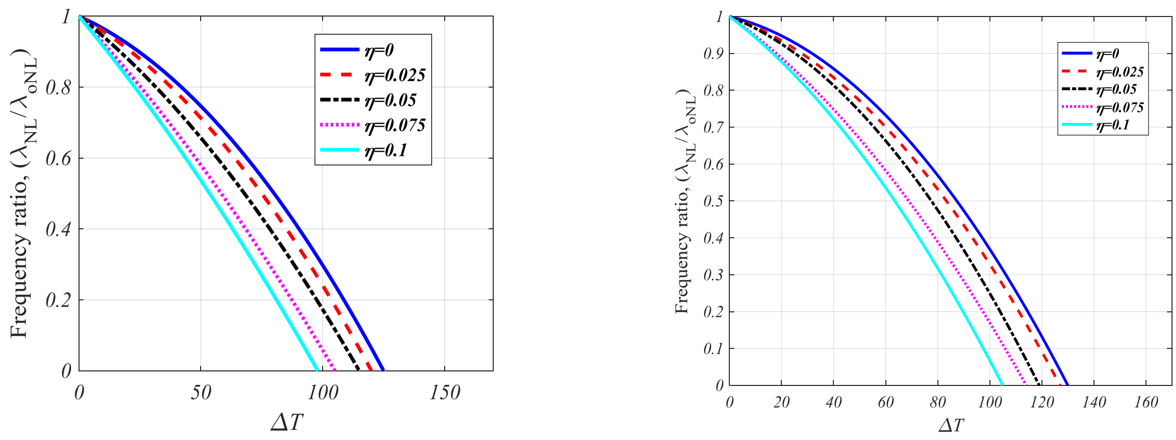

(a) Simple_simple

(b) Clamp_clamp

Fig. 24 Variation of the nonlinear frequency ratio with the temperature change for various values of the dimensionless length scale parameter.

amplitude of oscillations in linear mode. In other words, regardless of the nonlinear terms, the system's stiffness has been considered less than what it is, and the amplitude of fluctuations has been estimated more than what it actually is. Another interesting point which can be concluded from these figures is that with an increase in amplitude of the applied force, the differences between the results in linear and nonlinear modes will increase. The reason is that with an increase in amplitude of the applied force and the amplitude of fluctuations, nonlinear terms also become more significant and ignoring them will result in more errors. As it is specified Figs. 20(a)-(b), as the constraints of the system increases, i.e., in (C_C) mode, the differences between linear and nonlinear modes decrease. Figs. 21(a)-(b) shows the importance of studying the length scale parameter in microbeams, because with an increase in the scale parameter, oscillation amplitude decreases and the period decrease as well. As it is clear, when the body is more constrained, this effect will be greater and there will be less range of motion whit an increase in the length scale parameter. In Figs. 22(a)-(b), with an increase in the amplitude of force q0, the displacement also increases. Then we will discuss the effect of change in angle of orthotropic foundation on the amount of displacement with dynamic force (Figs. 23(a)-(b)). In this mode, as the angle increases, the displacement, force amplitude and also the period increase. As can be seen in forced vibrations, the force amplitude decreases over time and this is due to the effect of damping coefficient of foundation. With an increase in this coefficient, amplitude force decreases with time. Increasing in foundation coefficients including Winkler, nonlinear coefficient, and Pasternak lead to a reduction in displacement amplitude.

6.2.3 Changed temperature

In this example, materials whose mechanical and thermal properties are temperature-dependent are also studied. The nonlinear natural frequency, when the temperature changes are zero, is shown by λ_{0NL} and the nonlinear frequency ratio to λ_{0NL} is investigated. In Figs. 24(a)-(b), useful results are obtained from temperature and small scale parameter variations in terms of nonlinear frequency ratio. By increasing the length parameter, the effects of the rigidity matrix are reduced and the natural frequency decreases. As the temperature rises, the system is softened and decreases by decreasing the natural frequency hardness matrix.

7. Conclusions

In this paper a nonlinear Euler-Bernoulli beam model based on the nonlinear orthotropic visco-Pasternak foundation has been developed by using the modified couple stress theory. This nonclassic continuum theory is capable of prediction and explanation of size effects. In numerical examples, changes of the length scale parameter and foundation coefficients on the nonlinear frequency ratio and midpoint deflection of microbeam in free and forced vibration are presented that following results were obtained:

(1) The length scale parameter, which plays a major role in analysing the behaviour of microbeams, has been examined in this research. The results show that increasing the length scale parameter leads to an increase in nonlinear frequency; however, it reduces the frequency ratio. This displacement reflects the increased stiffness of the beam which is due to an increase in the length scale parameter.

(2) With an increase in Winkler, Pasternak and damping coefficients, frequency ratio decrease; moreover, the system becomes stiffer and nonlinear frequency increases.

(3) With an increase in nonlinear coefficients and orthotropic shear angle, frequency ratio increases and nonlinear frequency decreases which is due to an increase in softness of the system.

(4) As the radius of gyration increases, frequency ratio decreases and nonlinear frequency increases and the system becomes stiffer. As the charts and tables show with an increase in r (increasing the

thickness of beam), the difference between linear and nonlinear frequency reduces. In other words, when the beam is thinner and taller, ignoring the nonlinear effects will lead to more errors. However, with an increase in the initial displacement, i.e., $W_{\max}$, the opposite of this mode happens and the system becomes softer.

(5) With an increase in the amplitude of applied force, obviously, the beam oscillation amplitude will also increase oscillations amplitude in linear mode. In other words, ignoring the nonlinear terms considers the system's stiffness less than what it is and estimates the oscillations amplitude more than what it actually is. Therefore, with an increase in the amplitude of the applied force, the differences between the results in linear and nonlinear modes will increase. The reason is that with an increase in amplitude of the applied force and increase in the amplitude of oscillations, nonlinear terms also become more significant and ignoring them will lead to more errors.

(6) The comparison of linear and nonlinear analysis results has nicely confirmed that in linear mode, natural frequency (vibrations period) is completely independent of the initial conditions; however, in nonlinear mode, as the amplitude increases in the initial conditions, oscillation period reduces; in other words, the natural frequencies increase.

(7) The present study shows that in Euler-Bernoulli microbeam, with an increase in range of motion at the initial time, nonlinear frequency of the beam increases as well which represents the increase of the system's stiffness parallel to the increase in range of motion. This phenomenon indicates that, in practice, if for any reason the range of a system starts to increase, the system itself will resist against increase of the range by increasing its stiffness.

(8) Comparison of different boundary conditions indicate that in clamp, in order to observe and make a difference between linear and nonlinear modes, it is necessary to apply more force or much more initial displacement to the beam; in other words, when boundary conditions are more constrained, the linear solution can be considered acceptable in a broader range of initial conditions. In addition, whatever boundary conditions are freer, ignoring nonlinear terms will result in more errors

Acknowledgments

The authors wish to express their sincere thanks to the reviewers for their constructive for improving the paper. This work was supported by University of Kashan [Grant Number 574600/51].

References

Al-Basyouni, K.S., Tounsi, A. and Mahmoud, S.R. (2015), "Size dependent bending and vibration analysis of functionally graded micro beams based on modified couple stress theory and neutral surface position", *Compos. Struct.*, **125**, 621-630.

Azrar, L., Benamar, R. and White, R. (1999), "Semi-analytical approach to the non-linear dynamic response problem of S–S and C–C beams at large vibration amplitudes part I: General theory and application to the single mode approach to free and forced vibration analysis", *J. Sound Vib.*, **224**(2), 183-207.

Bellman, R. and Roth, R.S. (1979), "Systems identification with partial information", *J. Math. Anal. Appl.*, **68**(2), 321-333.

Bert, C.W. and Malik, M. (1996), "Differential quadrature method in computational mechanics: a review", *Appl. Mech. Rev.*, **49**, 1-28.

Eringen, A.C. and Edelen, D. (1972), "On nonlocal elasticity", *Int. J. Eng. Sci.*, **10**(3), 233-248.

Farokhi, H. and Ghayesh, M.H. (2015), "Thermo-mechanical dynamics of perfect and imperfect Timoshenko microbeams", *Int. J. Eng. Sci.*, **91**, 12-33.

Farokhi, H. and Ghayesh, M.H. (2017), "Viscoelasticity effects on resonant response of a shear deformable extensible microbeam", *Nonlinear Dyn.*, **87**(1), 391-406.

Ghayesh, M.H. and Amabili, M. (2014), "Coupled longitudinal-transverse behaviour of a geometrically imperfect micro-beam", *Compos. Part B: Eng.*, **60**, 371-377.

Ghayesh, M.H. and Farokhi, H. (2015), "Coupled longitudinal-transverse-rotational behaviour of shear deformable microbeams", *Compos. Part B: Eng.*, **77**, 319-328.

Ghayesh, M.H., Farokhi, H. and Amabili, M. (2013), "Nonlinear dynamics of a microscale beam based on the modified couple stress theory", *Compos. Part B: Eng.*, **50**, 318-324.

Ghayesh, M.H., Farokhi, H. and Amabili, M. (2014), "In-plane and out-of-plane motion characteristics of microbeams with modal interactions", *Compos. Part B: Eng.*, **60**, 423-439

Ghayesh, M.H., Farokhi, H. and Gholipour, A. (2017), "Oscillations of functionally graded microbeams", *Int. J. Eng. Sci.*, **110**, 35-53.

Ghorbanpour Arani, A., Mohammadimehr, M., Arefmanesh, A. and Ghasemi, A. (2010), "Transverse vibration of short carbon nanotubes using cylindrical shell and beam models", *Proceedings of the Institution of Mechanical Engineers Part C: Journal of Mechanical Engineering Science*, **224**(3), 745-756.

Ghorbanpour Arani, A. and Shokravi, M. (2013), "Nonlocal vibration behavior of a viscoelastic SLGS embedded on visco-Pasternak foundation under magnetic field", *J. Nanostruct.*, **3**(4), 467-476.

Ghorbanpour Arani, A., Kolahchi, R., Vossough, H. and Abdollahian, M. (2013), "Vibration and stability analysis of a Pasternak bonded double-GNR-system based on different nonlocal theories", *J. Solid Mech.*, **5**(1), 92-106.

Gurtin, M.E. and Ian Murdoch, A. (1975), "A continuum theory of elastic material surfaces", *Arch. Rational Mech. Anal.*, **57**(4), 291-323.

Jia, X.L., Ke, L.L., Feng, C.B., Yang, J. and Kitipornchai, S. (2015), "Size effect on the free vibration of geometrically nonlinear functionally graded micro-beams under electrical actuation and temperature change", *Compos. Struct.*, **133**, 1137-1148.

Kahrobaiyan, M., Rahaeifard, M., Tajalli, S. and Ahmadian, M. (2012), "A strain gradient functionally graded Euler–Bernoulli beam formulation", *Int. J. Eng. Sci.*, **52**, 65-76.

Ke, L.L., Wang, Y.S., Yang, J. and Kitipornchai, S. (2012), "Nonlinear free vibration of size-dependent functionally graded microbeams", *Int. J. Eng. Sci.*, **50**(1), 256-267.

Kong, S., Zhou, S., Nie, Z. and Wang, K. (2008), “The size-dependent natural frequency of Bernoulli–Euler micro-beams”, *Int. J. Eng. Sci.*, **46**(5), 427-437.
Kuang, J.H. and Chen, C.J. (2004), “Dynamic characteristics of shaped micro-actuators solved using the differential quadrature method”, *J. Micromech. Microeng.*, **14**(4), 647-655.
Lam, D.C., Yang, F., Chong, A., Wang, J. and Tong, P. (2003), “Experiments and theory in strain gradient elasticity”, *J. Mech. Phys. Solids*, **51**(8), 1477-1508.
Lyshevski, S.E. (2002), *MEMS and NEMS: Systems, Devices, and Structures*, (1th Edition), CRC press, New York, NY, USA.
Ma, H., Gao, X.L. and Reddy, J. (2010), “A nonclassical Reddy-Levinson beam model based on a modified couple stress theory”, *Int. J. Multiscale Computat. Eng.*, **8**(2), 217-235.
Mohammadimehr, M. and Shahedi, S. (2016), “Nonlinear magneto-electro-mechanical vibration analysis of double-bonded sandwich Timoshenko microbeams based on MSGT using GDQM”, *Steel Compos. Struct., Int. J.*, **21**(1), 1-36.
Mohammadimehr, M., Rostami, R. and Arefi, M. (2016), “Electro-elastic analysis of a sandwich thick plate considering FG core and composite piezoelectric layers on Pasternak foundation using TSDT”, *Steel Compos. Struct., Int. J.*, **20**(3), 513-543.
Newmark, N.M. (1959), “A method of computation for structural dynamics”, *J. Eng. Mech. Div.*, **85**(3), 67-94.
Park, W.T., Han, S.C., Jung, W.Y. and Lee, W.H. (2016), “Dynamic instability analysis for S-FGM plates embedded in Pasternak elastic medium using the modified couple stress theory”, *Steel Compos. Struct., Int. J.*, **22**(6), 1239-1259.
Peng, J., Yang, L., Lin, F. and Yang, J. (2017), “Dynamic analysis of size-dependent micro-beams with nonlinear elasticity under electrical actuation”, *Appl. Math. Model.*, **43**, 441-453.
Rashvand, K., Rezazadeh, G., Mobki, H. and Ghayesh, M.H. (2013), “On the size-dependent behavior of a capacitive circular micro-plate considering the variable length-scale parameter”, *Int. J. Mech. Sci.*, **77**, 333-342.
Rahmani, O., Refaeinejad, V. and Hosseini, S.A.H. (2017), “Assessment of various nonlocal higher order theories for the bending and buckling behavior of functionally graded nanobeams”, *Steel Compos. Struct., Int. J.*, **23**(3), 339-350.
Rao, S.S. (2007), *Vibration of Continuous Systems*, John Wiley & Sons, New Jersey, Inc., USA.
Reddy, J.N. (2002), *Energy Principles and Variational Methods in Applied Mechanics*, John Wiley & Sons, New Jersey, Inc., USA.
Roque, C., Fidalgo, D., Ferreira, A. and Reddy, J. (2013), “A study of a microstructure-dependent composite laminated Timoshenko beam using a modified couple stress theory and a meshless method”, *Compos. Struct.*, **96**, 532-537.
Sahmani, S., Bahrami, M., Aghdam, M. and Ansari, R. (2014), “Surface effects on the nonlinear forced vibration response of third-order shear deformable nanobeams”, *Compos. Struct.*, **118**, 149-158.
Simsek, M. (2011), “Forced vibration of an embedded single-walled carbon nanotube traversed by a moving load using nonlocal Timoshenko beam theory”, *Steel Compos. Struct., Int. J.*, **11**(1), 59-76.
Şimşek, M. (2014), “Nonlinear static and free vibration analysis of microbeams based on the nonlinear elastic foundation using modified couple stress theory and He’s variational method”, *Compos. Struct.*, **112**, 264-272.
Stölken, J. and Evans, A. (1998), “A microbend test method for measuring the plasticity length scale”, *Acta Materialia*, **46**(14), 5109-5115.
Tagrara, S.H., Benachour, A., Bouiadjra, M.B. and Tounsi, A. (2015), “On bending, buckling and vibration responses of functionally graded carbon nanotube-reinforced composite beams”, *Steel Compos. Struct., Int. J.*, **19**(5), 1259-1277.
Tilmans, H.A. and Legtenberg, R. (1994), “Electrostatically driven vacuum-encapsulated polysilicon resonators: Part II. Theory and performance”, *Sensor. Actuat. A: Phys.*, **45**(1), 67-84.
Wang, Y.G., Lin, W.H. and Liu, N. (2013), “Nonlinear free vibration of a microscale beam based on modified couple stress theory”, *Physica E: Low-dimensional Syst. Nanostruct.*, **47**, 80-85.
Yang, F., Chong, A.C., Lam, D.C.C. and Tong, P. (2002), “Couple stress based strain gradient theory for elasticity”, *Int. J. Solids Struct.*, **39**(10), 2731-2743.
Yang, J., Hu, Y. and Kitipornchai, S. (2012), “Electro-dynamic behavior of an electrically actuated micro-beam: Effects of initial curvature and nonlinear deformation”, *Comput. Struct.*, **96**, 25-33.
Zhong, H. and Guo, Q. (2003), “Nonlinear vibration analysis of Timoshenko beams using the differential quadrature method”, *Nonlinear Dyn.*, **32**(3), 223-234.

CC

Appendix A

According to the differential quadrature rule, derivatives of a function in $x = x_i$ is expressed in terms of the value of function in throughout domain as

$$\left.\frac{d^r f}{dx^r}\right|_{x=x_i} = \sum_{j=1}^{N} A_{ij}^{(r)} f_j , \tag{35}$$

where $A^{(r)}$ are the weighting coefficients associated with the rth order derivative and N is the number of grid points in the x-direction. These coefficients for the first-order derivatives are given by Bellman and Roth (1979)

$$A_{ij}^{(1)} = \begin{cases} \dfrac{\prod\limits_{\substack{m=1\\ m\neq i,j}}^{N}(x_i - x_m)}{\prod\limits_{\substack{m=1\\ m\neq j}}^{N}(x_j - x_m)}, & (i, j = 1,2,3,\ldots,N; i \neq j) \\ \sum\limits_{\substack{m=1\\ m\neq i}}^{N} \dfrac{1}{x_i - x_m}, & (i = j = 1,2,3,\ldots,N) \end{cases} . \tag{36}$$

The weighting coefficients of higher-order derivatives are extracted from the following recurrence relation

$$\left[A^{(r)}\right] = \left[A^{(1)}\right]\left[A^{(r-1)}\right] \tag{37}$$

A convenient choice for the grid points are the equally spaced points. Another option which gives more accurate results is unequally spaced grid points. A well-accepted set of the grid points is the Gauss–Lobatto–Chebyshev points given for interval [0, L] by

$$\bar{x}_i = \frac{x_i}{L} = \frac{1}{2}\left\{1 - \cos[\frac{(i-1)\pi}{(N-1)}]\right\}, \ (i = 1,2,3,\ldots,N). \tag{38}$$

The main advantage of this set is compression of the points in two ends which provides high accuracy in estimation of the value of the derivatives of function in the boundary points. When the desired function has nonlinear derivatives, Eq. (35) can be expressed as follows (Kuang and Chen 2004)

$$\left.(\frac{df}{dx})^2\right|_{x=x_i} = \sum_{j=1}^{N} A_{ij}^{(1)} y_j \,\Theta \sum_{j=1}^{N} A_{ij}^{(1)} y_j \tag{39}$$

Where Θ represents Hadamard multiplication.

Appendix B

Table 3 types of boundary conditions

Dimensionless B.C		Boundary conditions
$U=0$ $W=0$ $\frac{\partial W}{\partial \zeta}=0$		Clamp (C)
$U=0$ $W=0$ $\frac{\partial^2 W}{\partial \zeta^2}=0$		Simply supported (non-sliding) (S)
$\frac{\partial U}{\partial \zeta}+\frac{1}{2}\left(\frac{\partial W}{\partial \zeta}\right)^2-\alpha\Delta T=0$ $W=0$ $\frac{\partial^2 W}{\partial \zeta^2}=0$		Simply supported (sliding) (S^*)
$U=0$ $\frac{\partial^3 W}{\partial \zeta^3}+K_p\cos(\theta)\frac{\partial W}{\partial \zeta}=0$ $\frac{\partial W}{\partial \zeta}=0$		Hinged (H)
$\frac{\partial U}{\partial \zeta}+\frac{1}{2}\left(\frac{\partial W}{\partial \zeta}\right)^2-\alpha\Delta T=0$ $\frac{\partial^3 W}{\partial \zeta^3}+K_p\cos(\theta)\frac{\partial W}{\partial \zeta}=0$ $\frac{\partial^2 W}{\partial \zeta^2}=0$		Free (F)